Analytical Methods

Accepted Manuscript

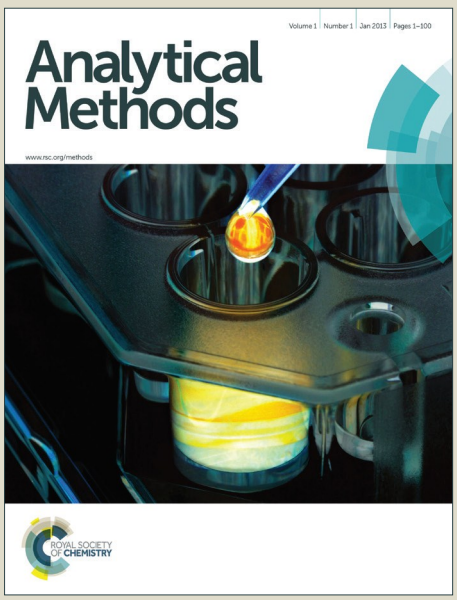

This is an *Accepted Manuscript*, which has been through the Royal Society of Chemistry peer review process and has been accepted for publication.

Accepted Manuscripts are published online shortly after acceptance, before technical editing, formatting and proof reading. Using this free service, authors can make their results available to the community, in citable form, before we publish the edited article. We will replace this *Accepted Manuscript* with the edited and formatted *Advance Article* as soon as it is available.

You can find more information about *Accepted Manuscripts* in the Information for Authors.

Please note that technical editing may introduce minor changes to the text and/or graphics, which may alter content. The journal's standard Terms & Conditions and the Ethical guidelines still apply. In no event shall the Royal Society of Chemistry be held responsible for any errors or omissions in this *Accepted Manuscript* or any consequences arising from the use of any information it contains.

ROYAL SOCIETY OF CHEMISTRY

www.rsc.org/methods

Cite this: DOI: 10.1039/c0xx00000x

www.rsc.org/xxxxxx

ARTICLE TYPE

Simultaneous determination of dopamine, ascorbic acid and uric acid using multi-walled carbon nanotubes and reduced graphene oxide hybrid functionalized by PAMAM and Au nanoparticles

Siyuan Wang, Wen Zhang, Xia Zhong, Yaqin Chai,* Ruo Yuan*

Received (in XXX, XXX) Xth XXXXXXXXX 20XX, Accepted Xth XXXXXXXXX 20XX
DOI: 10.1039/b000000x

A nanohybrid based on reduced graphene oxide functionalized by poly(amido-amine), multi-walled carbon nanotubes and Au nanoparticles (RGO-PAMAM-MWCNTs-AuNPs) for simultaneous electrochemical determination of ascorbic acid (AA), dopamine (DA) and uric acid (UA) was reported in this paper. The RGO-PAMAM-MWCNTs-AuNPs-modified electrode showed a high selectivity towards the oxidation of AA, DA, and UA, and resolve their overlapped oxidation peaks into three well-defined peaks. The RGO-PAMAM-MWCNTs-AuNPs nanohybrids were characterized by scanning electron microscopy (SEM). Several important parameters that control the performance of the electrochemical sensor were investigated and optimized. Under the optimal condition with differential pulse voltammetry (DPV) method, the linear response ranges for the determination of AA, DA, and UA are 20 μM~1.8 mM, 10 μM~0.32 mM, and 1 μM~0.114 mM in the co-existence systems, respectively. The corresponding detection limits are 6.7 μM, 3.3 μM and 0.33 μM (S/N = 3), respectively.

Introduction

It is well known that ascorbic acid (AA), dopamine (DA) and uric acid (UA) always coexist in the extra cellular fluids of central nervous system and serum in mammals, and they are crucial molecules for physiological reactions in human metabolism. In detail, as a common anti-oxidant, AA plays a great role in the metabolic process of human bodies. It can efficiently scavenge toxic free radicals and other reactive oxygen species formed in cell metabolism [1-3]. DA plays a valuable part in renal, hormonal, cardiovascular and central nervous systems. Lack of DA would result in neurological disorders such as Parkinson's disease and schizophrenia [4-6]. UA is the main final product of purine metabolism in the human body. Abnormal concentration levels of UA indicate some diseases, such as gout, hyperuricaemia and Lesch-Nyan syndrome [7,8]. In the past half century, electrochemical techniques have led to considerable interest for detection and quantification of AA, DA and UA, due to their rapid response, high sensitivity, low expense and simple operation [9]. Nevertheless, AA and UA normally exist together with DA in biological samples, and they are oxidized at nearby potentials [10]. Therefore, it is highly difficult to achieve their simultaneous detection.

To simultaneously detect AA, DA and UA, various materials such as polymers, carbon materials and metal complexes have been used to modify electrodes [9]. Among them, carbon-based nanomaterials such as graphene and carbon nanotubes (CNTs) are the most widely used as modifiers, due to their large electrochemical active surface area and good catalytic activity [11-15]. But owing to the π-π interaction between individual graphene, graphene is easy to form irreversible agglomerates or even restock to form graphite. The long and tortuous multi-walled carbon nanotubes (MWCNTs) can bridge adjacent graphene to restrain their aggregation efficiently [16]. Besides, only MWCNTs or graphene modified electrode can not detect AA and DA selectively [8-10,17], so it is necessary to functionalize carbon materials. For instance, boron-doped carbon nanotubes were used to modify glassy carbon electrode (GCE) as sensitive method for detecting dopamine [18]. Besides, Bao and co-workers reported an electrochemical method for simultaneous detection of AA, DA and UA based on the graphene oxide-templated polyaniline microsheets [19].

Recent years, dendrimers have been studied in the presence of metal nanoparticles in both aqueous and nonaqueous systems [20-23]. Among various dendrimers, poly(amido-amine) (PAMAM) dendrimers are the most frequently studied one [24]. PAMAM dendrimers are the regular tree-like highly branched macromolecules, which have multiple branch ends available for further synthesis. Besides, PAMAM dendrimers have unique properties such as a high density of active groups, good structural homogeneity and good biocompatibility [25-29]. The combination of metal nanoparticles with PAMAM can prevent the aggregation of metal nanoparticles [30,31]. PAMAM and cysteamine-capped gold nanoparticles (AuNPs) have been used to modify GCE for detecting UA in human serum without AA interference [32].

Based on above observation, herein, PAMAM and AuNPs are used to functionalize reduced graphene oxide (RGO) and

Key Laboratory of Luminescence and Real-time Analytical Chemistry, Ministry of Education, College of Chemistry and Chemical Engineering, Southwest University, Chongqing, 400715, People's Republic of China. E-mail: yqchai@swu.edu.cn (Y.Q. Chai), yuanruo@swu.edu.cn (R.Yuan); Fax: +86-23-68253172; Tel: +86-23-68252277

MWCNTs to form a nanohybrid (RGO-PAMAM-MWCNTs-AuNPs) for the simultaneous electrochemical determination of AA, DA and UA. This strategy provides an efficient and promising platform for the sensing devices due to the integration of the excellent performance of AuNPs, PAMAM dendrimers, RGO and MWCNTs.

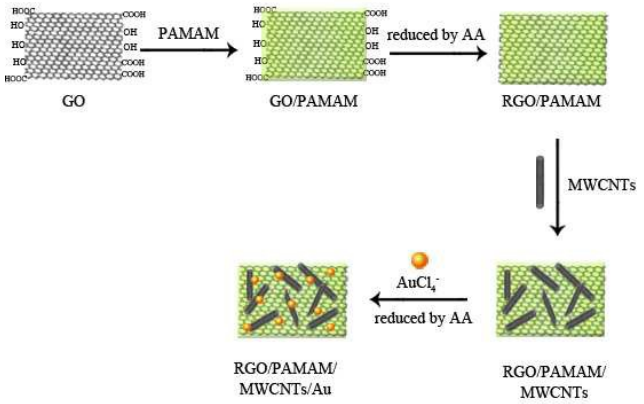

Scheme 1. Preparation of RGO-PAMAM-MWCNTs-AuNPs nanohybrid material.

Experimental methods

Chemicals

Graphene oxide (GO) was purchased from Nanjing Xianfeng nano Co. (Nanjing, China). Multi-walled carbon nanotubes (MWCNTs, 95% purity) were supplied by Chengdu Orangic Chemicals Co. Ltd. of the Chinese Academy of Science (Chengdu, China). Gold chloride ($HAuCl_4$) and dopamine (DA) were obtained from Sigma Chemical (St. Louis, MO, USA). Ascorbic acid (AA) and uric acid (UA, 99% purity) were obtained from Aladdin Chemistry Co. Ltd (Chengdu, China). Poly(amido-amine) dendtimer (PAMAM, G3.5-COOH) was purchased from Weihai CY Dendrimer technology Co. Ltd. (Weihai, China). Other chemicals and solvents were of analytical grade and used as received. Ultrapure water (specific resistance of 18.2 M Ω cm) was used throughout this study. Phosphate-buffered solutions (PBS 0.1 M) at various pH were prepared using 0.10 M Na_2HPO_4 and 0.10 M NaH_2PO_4. The supporting electrolyte was 0.10 M KCl.

Apparatus

Electrochemical measurements were carried out with a CHI660A electrochemical workstation (Shanghai Chenhua Instrument, Co., China).The three-compartment electrochemical cell contained a modified GCE (Φ=4 mm) as the working electrode, a saturated calomel electrode (SCE) as reference electrode, and a platinum wire as auxiliary electrode. The surface morphologies were evaluated by scanning electron microscopy (SEM S-4800, Hitachi, Japan). All measurements were carried out at room temperature.

Preparation of RGO-PAMAM-MWCNTs-AuNPs nanohybrid material

The hybrid material was prepared as follows. Firstly, 2 mg GO was dispersed in 2 mL ultrapure water. 50 μL PAMAM solution (1 mg/mL) was added, and the mixture solution was subjected to ultrasonic condition for 10 min and then continually stirred over night at room temperature. By this step, the resulting mixture solution turned from transpicuous to non-transparent. Next, the mixture was heated to 60 □ under continual stirring. Then 4 mL AA solution containing 0.084 g AA was added into the mixture. After 12 h, the color of mixture changed from dark yellow to black, indicating that reduced graphene oxide-PAMAM (RGO-PAMAM) compound was synthesized. The production was centrifuged and washed using ultrapure water. The sediment was resuspended in ultrapure water and 2 mL MWCNTs suspension (1 mg/mL) was dropped into the solution to form a homogeneous suspension under ultrasonic condition for 30 min and stirring for 2 h. Subsequently, 100 μL 1% $HAuCl_4$ was added in the mixture under continual stirring for 30 min. Then, AA solution was added dropwise. After heated in water bath to 60□ for another 12 h under continual stirring, the mixture was centrifuged and washed to obtain RGO-PAMAM-MWCNTs-AuNPs, which was resuspended in ultrapure water and stored at 4 ℃ for further use. Other compared materials including RGO, RGO-PAMAM and RGO-PAMAM-Au nanoparticles (RGO-PAMAM-AuNPs) were prepared with similar method.

Fabrication of the sensor

A GCE was polished to a mirror-like finish with 0.3 and 0.05 μm alumina powder, and further sonicated in ethanol and ultrapure water, respectively, then dried at room temperature. 10 μL the suspension of RGO-PAMAM-MWCNTs-AuNPs was dropped onto the surface of the pretreated GCE and dried in air for 8 h to obtain RGO-PAMAM-MWCNTs-AuNPs/GCE.

Results and discussion

SEM characterization

The morphology and microstructure of as-prepared hybrids and the material were characterized using SEM (Fig. 1). As shown in Fig. 1a, the image of RGO presents sheet and wrinkled structure. Fig. 1b displays the SEM of RGO-PAMAM and a misty film on the sheet of RGO was observed, indicating the formation of RGO-PAMAM composite. Bright nanoparticles were observed at the SEM image of RGO-PAMAM-AuNPs (Fig. 1c) and their sizes were in the range from 50 to 200 nm, confirming that AuNPs are successfully synthesized on RGO-PAMAM composite. The SEM image of RGO-PAMAM-MWCNTs-AuNPs is exhibited in Fig. 1d. The gray lamellar structure belongs to RGO-PAMAM composite, which was fully covered by MWCNTs, and the bright rotundity spots on both MWCNTs and RGO were the modified AuNPs.

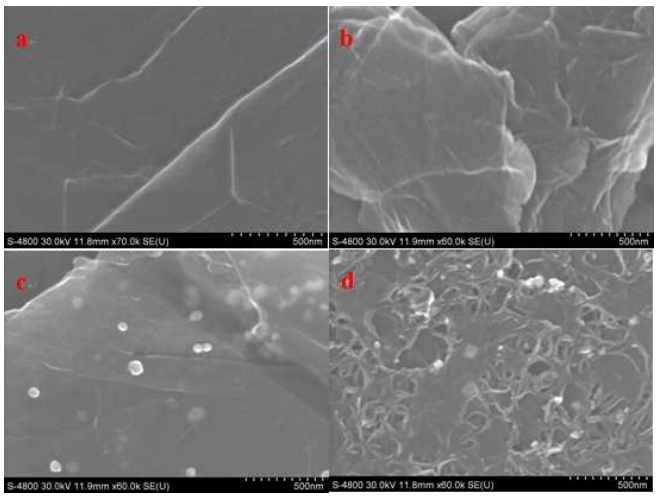

Fig. 1. SEM images of RGO (a), RGO-PAMAM (b), RGO-PAMAM-AuNPs (c) and RGO-PAMAM-MWCNTs-AuNPs (d).

Optimization of detection conditions

The pH of the working buffer is very important for the detection of AA, DA and UA, because the protons took part in the electrode reaction. The influence of pH on the oxidation of AA (500 μM), DA (70 μM) and UA (20 μM) was investigated by differential pulse voltammetry (DPV). From Fig. 2a, we can see the effect of pH on the peak current. At pH 4.0, the peak currents of AA and UA are the highest value. Furthermore, the current resonpse of DA is also strong at this pH. Fig. 2b displays the influence of pH on the peak potentials. As shown, all peak potentials of AA, DA and UA decreased with the increase of pH. Fig. 2c shows the change of the peak sparations of DA-AA and UA-DA *vs.* the pH. As observed, the sparations between the peak potentials of DA-AA and UA-DA were large enough to achieve the simultaneous determination of three analytes at pH 4.0. Considering the influence of pH on both the peak currents and the peak separations, pH 4.0 was chosen as the optimal pH for further experiments. Additionally, the volume of RGO-PAMAM-MWCNTs-AuNPs suspension dropped onto GCE was also optimized (data not shown). The electrode modified with 10 μL of suspension exhibited the best performance when compared to that in the case of 8 μL and 15 μL of suspension. Thus, 10 μL of suspension was used to modify the electrode.

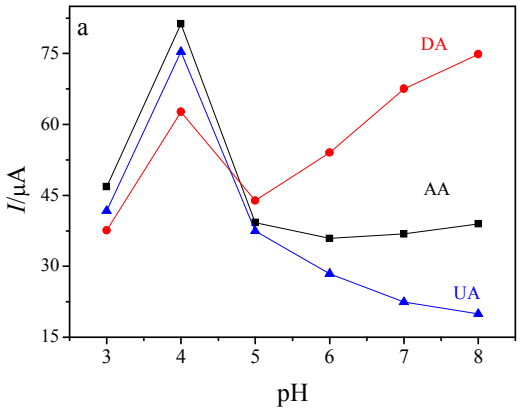

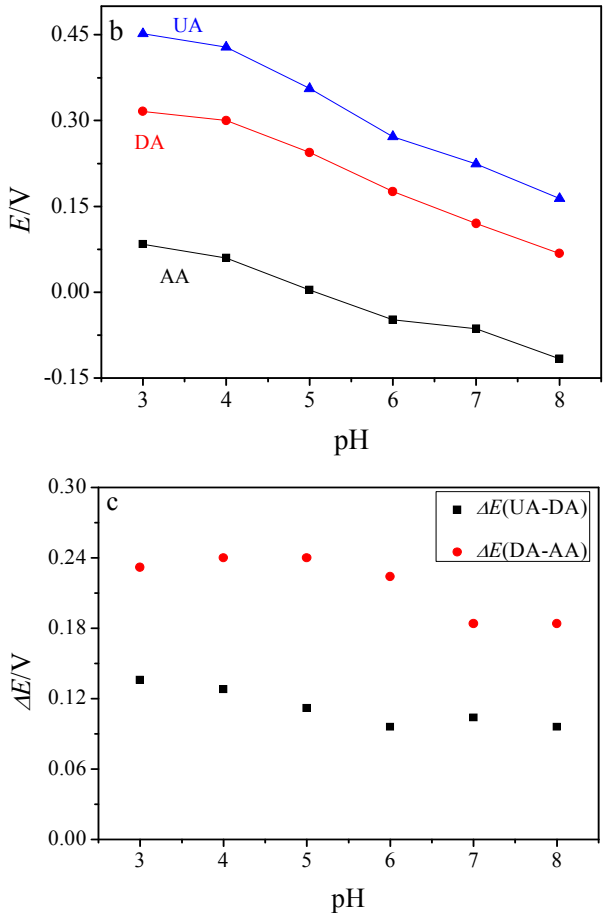

Fig. 2. Effect of pH on (a) the peak current and (b) the peak potential for the oxidation of 500 μM AA, 70 μM DA, 20 μM UA in 0.1 M PBS (pH 4.0). (c) The peak sparations of DA-AA and UA-DA vs. the pH.

DPV behaviors of AA, DA and UA at the modified electrode

Fig. 3 displays the differential pulse voltammetry of AA, DA and UA at bare GCE (a), RGO/GCE (b), RGO-PAMAM-AuNPs/GCE (c) and RGO-PAMAM-MWCNTs-AuNPs/GCE (d), respectively. At the bare GCE, only two broad oxidation peaks were observed, indicating that it is impossible to simultaneous determination of AA and DA on bare GCE. For RGO modified electrode, the peak of UA was at 0.5 V, but the peaks of AA and DA were at same potential (0.36 V). At RGO-PAMAM-AuNPs/GCE, the oxidation peaks of DA and UA were observed at 0.36 V and 0.49 V, respectively, while the oxidation peak of AA was unconspicuous and smaller. However, at RGO-PAMAM-MWCNTs-AuNPs modified GCE, the peaks of AA, DA and UA appeared at 0.06 V, 0.30 V, 0.43 V, respectively, indicating that it is possible to achieve the simultaneous determination of AA, DA and UA. It can be considered that this RGO-PAMAM-MWCNTs-AuNPs nanohybrid formed a 3D hierarchical structure, which is caused by 1D MWCNTs and 2D RGO. MWCNTs effectively inhibited the stacking of individual graphene and enhanced the utilization of RGO-based composites. PAMAM (3.5G) molecules have a large amount of carboxylic functional groups that could provide a selective interface via hydrogen bonds with the proton-donating group of AA, DA and

UA.

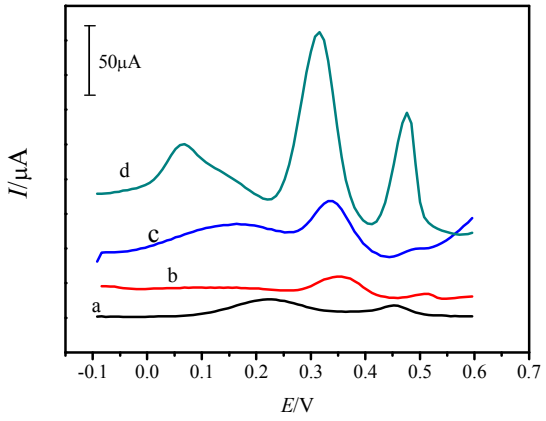

Fig. 3. DPV curves of bare GCE (a), RGO/GCE (b), RGO-PAMAM-AuNPs/GCE (c) and RGO-PAMAM-MWCNTs-AuNPs/GCE (d) in 0.1 M PBS (pH 4.0) containing 0.50 mM AA, 0.05 mM DA, 0.05 mM UA.

Investigation of the different ratios among MWCNTs, RGO, PAMAM and AuNPs

In order to investigate the cyclic voltammetry (CV) responses of the nanohydris with different ratios among MWCNTs, RGO, PAMAM and AuNPs towards simultaneous detection of AA, DA and UA, a variety of composites were synthesised. The detailed ratios of different nanohydrids are mentioned in Table 1.

Table 1 Chemicals ratio of different nanohydrids.

nanohydrids	GO/ mg	PAMAM(1mg /mL)/μL	MWCHTs/ mg	$HAuCl_4$ (1%)/μL
a	2	50	2	100
b	1	25	2	100
c	2	100	2	100
d	2	50	2	50
e	2	50	5	200
f	2	50	1	100

The morphology and microstructure of the nanohydrids with different ratios were characterized using SEM (Fig. 4). The SEM images (a-f) suggested that the nanohydrids (a-f) were successfully synthetized, respectively. The CV responses of nanohydrids (a-f) towards coexisting AA (1.00 mM), DA (0.30 mM) and UA (0.40 mM) were displayed in Fig. 5. Curves (a-f) are the CV responses of nanohydrids (a-f) modified GCE, respectively. As seen in curve (a), three oxidation peaks were separated enough to simultaneously detect three analytes. Furthermore, the peak currents are higher than other cases. Thus, the RGO-PAMAM-MWCNTs-AuNPs at the ratio (a) exhibited better performance on simultaneous determination of AA, DA and UA than those at other ratios.

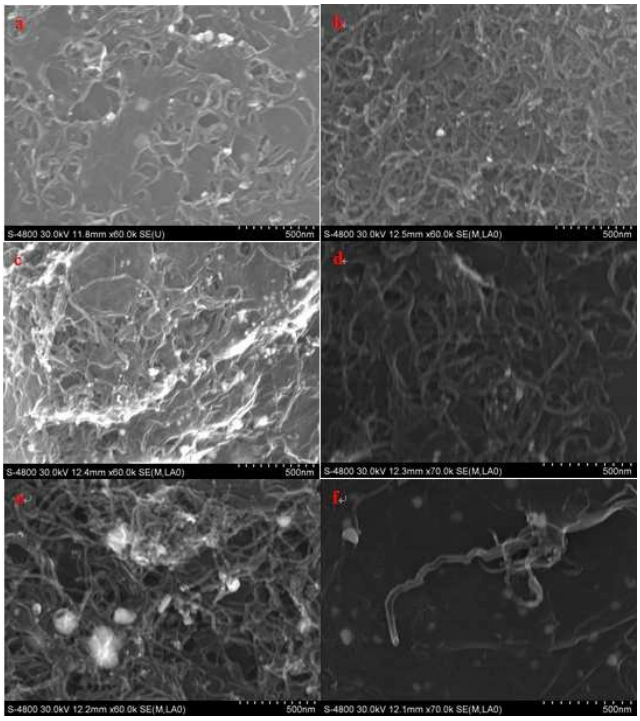

Fig. 4. SEM images of the different ratios (a-f) (in Table 1) among MWCNTs, RGO, PAMAM and AuNPs.

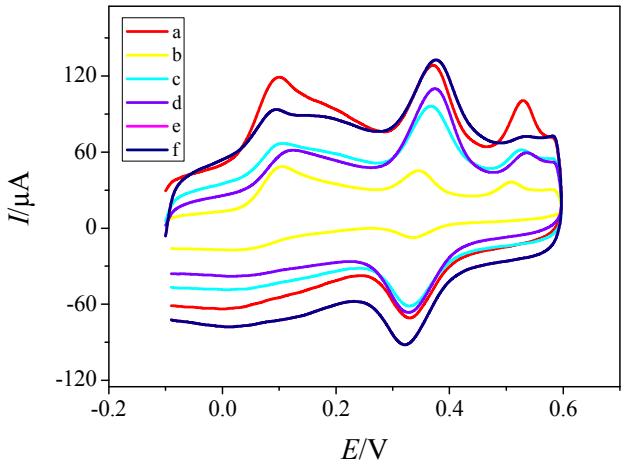

Fig. 5. Cyclic voltammograms of different nanohydrids (a-f) modified GCE containing 1.00 mM AA, 0.30 mM DA and 0.40 mM UA in PBS (pH 4.0).

Simultaneous detection of AA, DA and UA

The primary aim of the present investigation is to simultaneously determine AA, DA and UA. Fig. 6 displays the DPV curves of different concentrations of AA, DA and UA in the mixture at the RGO-PAMAM-MWCNTs-AuNPs modified electrode. The three well-separated peaks were obtained, and the peak currents increased with increasing the concentration of AA, DA and UA under optimization of detection conditions. The anodic peak potentials for AA, DA and UA were observed at 0.06, 0.32 and 0.44 V in the mixture, respectively. Meanwhile a wide peak between 0.1 V and 0.2 V was observed and it was attributed to the

the nanohydrid material. In fact, this back signal has no influence on the simultaneous determination three analytes. Hence, the experiment results indicated that it is possible to achieve the simultaneous detection of AA, DA and UA in the mixture solution.

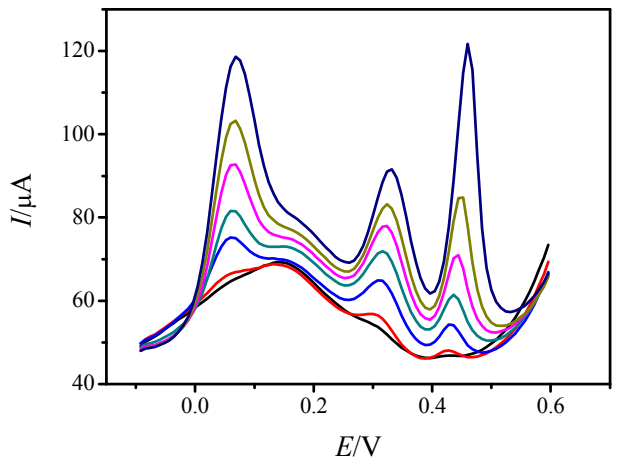

Fig. 6. DPV curves of the sensor in 0.1 M PBS (pH 4.0) containing individual concentration of AA, DA and UA mixture. [AA]: 0.03, 0.11, 0.19, 0.26, 0.36, 0.56 and 0.76 mM. [DA]: 10, 30, 50, 70, 110, 150 and 190 μM. [UA]: 1.5, 3.5, 7.5, 11.5, 21.5, 31.5 and 51.5 μM.

In three-fold mixture, the electro-oxidation processes of AA, DA and UA in the mixture were also investigated when the concentration of one species changed, meanwhile those of other two species are kept constant. Fig. 7 presents the DPV curves at different concentrations of AA, DA and UA in the presence of other species kept in constant, respectively. Fig. 7a illustrated the DPV response of AA at the sensor in the presence of DA (70 μM) and UA (10 μM). The linear regression equation was expressed as I (μA)=51.52+43.13c_{AA} (mM) and correlation coefficient of R^2_{AA}=0.994. The linear response range for AA was 20 μM~1.8 mM. As shown in Fig. 7b, the peak current of DA increases linearly with the increase in DA concentration from 10 μM to 0.32 mM in the mixture of AA (0.2 mM) and UA (6 μM). The linear regression equation was I (μA)=50.84+168.46c_{DA} (mM) and correlation coefficient of R^2_{DA}=0.995. Fig. 8c depicted the DPV response of UA in the presence of AA (0.2 mM) and DA (50 μM), which indicated a linear relationship in the concentration range of 1 μM~0.114 mM. the linear regression equation was expressed as I (μA)=45.36+940.61c_{UA} (mM) and the correlation coefficient of R^2_{UA}=0.993. In addition, the detection limit of AA, DA and UA were found to be 6.7 μM, 3.3 μM and 0.33 μM (S/N = 3), respectively. These results strongly suggest that AA, DA and UA can be selectively and sensitively determined at the proposed sensor in their ternary mixture. Compared with other reported methods (Table 2), this work exhibited wide linear response ranges and low detection limits for simultaneous detection of AA, DA and UA. The reasons may be ascribed as follows: (1) RGO and MWCNTs have large electrochemical active surface area, chemical stability and good catalytic activit. (2) PAMAM (3.5G) molecules possess a large amount of carboxylic functional groups, which could provide a selective interface via hydrogen bonds with the proton-donating group of AA, DA and UA. (3) MWCNTs dramatically enlarged the peak separation among AA, DA and UA and made the surface of the electrode more porous. (4) the conducting porous layers may be beneficial to the discrimination of many oxidize or reduce species at similar potentials. In summary, the modified electrode illustrated high sensitivity, selectivity and catalytic activity to simultaneous detection of AA, DA and UA.

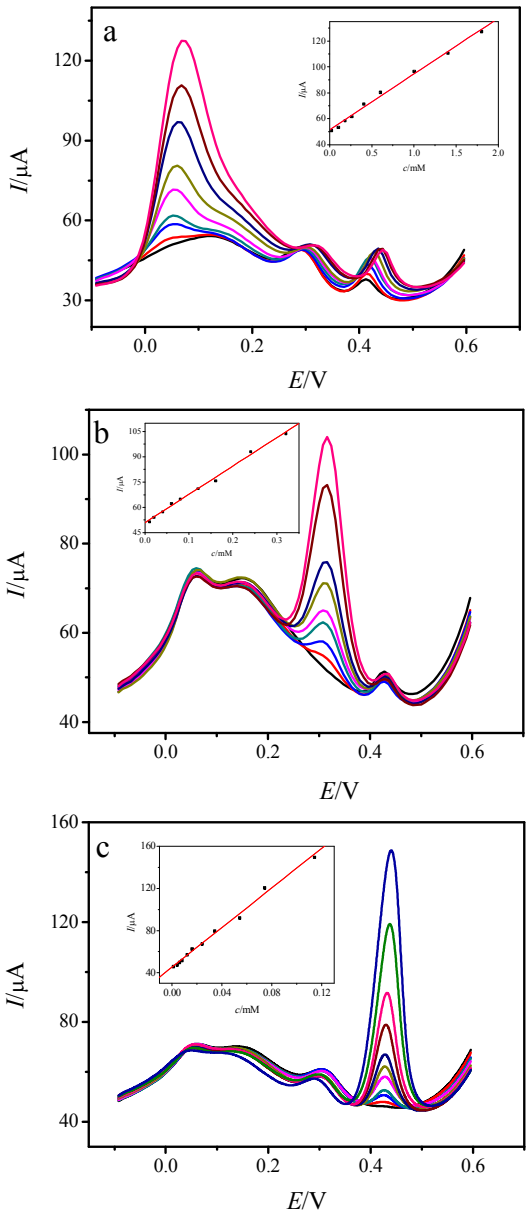

Fig. 7. DPV curves at the sensor in 0.1 M PBS (pH 4.0) (a) containing 70 μM DA, 10 μM UA and different concentrations of AA (from inner to outer): 0.02, 0.10, 0.18, 0.26, 0.40, 0.60, 1.00, 1.40, 1.80 mM; (b) containing 0.2 mM AA, 6 μM UA and different concentrations of DA (from inner to outer): 0.01, 0.02, 0.04, 0.06, 0.08, 0.12, 0.16, 0.24, 0.32 mM; (c) containing 0.2 mM AA, 50 μM DA and different concentrations of UA (from inner to outer): 0.001, 0.004, 0.006, 0.008, 0.012, 0.016, 0.024, 0.034, 0.054, 0.074, 0.114 mM, respectively.

Conclusions

In this work, a nanohybrid based on RGO functionalized by PAMAM and MWCNTs and AuNPs was utilized to modify GCE for simultaneous electrochemical determination of AA, DA and UA. The modified electrode resolved their overlapped oxidation peaks into three well-defined peaks through DPV technique. Due to the intergration of RGO, PAMAM, MWCNTs and AuNPs, the sensor showed a high selectivity towards the oxidation of AA, DA, and UA. The RGO-PAMAM-MWCNTs-AuNPs nanohybrid material would provide an efficient and promising platform for the sensing devices.

Acknowledgements

This work was financially supported by the NNSF of China (21075100, 21275119, 21105081), Ministry of Education of China (Project 708073), Natural Science Foundation of Chongqing City (CSTC-2011BA7003, CSTC-2010BB4121), State Key Laboratory of Silkworm Genome Biology (sklsgb2013012), the Doctor Foundation of Southwest University (swu113029) and the Fundamental Research Funds for the Central Universities (XDJK2013C115, XDJK2013A008, XDJK2013A27), China.

Notes and references

1 B.B. Xu, Q.J. Song, H.J. Wang, *Anal. Methods*, 2013, **5**, 2335.
2 L. Yang, D. Liu, J. Huang, T. You, *Sens. Actuators B,* 2014, **193**, 166.
3 O. Arrigoni, M.C. De Tullio, *BBA-Gen Subjects,* 2002, **1569**, 1.
4 N.G. Shang, P. Papakonstantinou, M. McMullan, M. Chu, A. Stamboulis, A. Potenza, S.S. Dhesi, H. Marchetto, *Adv. Funct. Mater.,* 2008, **18,** 3056.
5 C.R. Raj, T. Okajima, T. Ohsaka, *J. Electroanal. Chem*, 2003, **543**, 127.
6 D. Wu, Y. Li, Y. Zhang, P. Wang, Q. Wei, B. Du, *Electrochim. Acta,* 2014, **116**, 244.
7 P.K. Aneesh, S.R. Nambiar, T.P. Rao, A. Ajayaghosh, *Anal. Methods*, 2014, **6**, 5322.
8 W. Zhang, R. Yuan, Y.Q. Chai, Y. Zhuang, S.H. Chen, *Sens. Actuators B*, 2012, **166**, 601.
9 W. Zhang, Y.Q. Chai, R. Yuan, S.H. Chen, J. Han, D.H. Yuan, *Anal. Chim. Acta,* 2012, **756**, 7.
10 C. Wang, R. Yuan, Y. Chai, S.H. Chen, Y. Zhang, F. Hu, M. Zhang, *Electrochim. Acta*, 2012, **62**, 109.
11 S.H. Xie, Y.Y. Liu, J.Y. Li, *Appl. Phys. Lett.,* 2008, **92**, 243121..
12 H.J. Zhang, P.B. Gai, R. Cheng, L. Wu, X.H. Zhang, J.H. Chen, *Anal. Methods*, 2013, **5**, 3591.
13 M. Noroozifar, M. Khorasani-Motlagh, R. Akbari, M.B. Parizi, *Biosens. Bioelectron.*, 2011, **28**, 56.
14 M. Zhou, Y.M. Zhai, S.J. Dong, *Anal. Chem.*, 2009, **81**, 5063.
15 C.L. Suna, H.H. Leea, J.M. Yanga, C.C. Wub, *Biosens. Bioelectron.*, 2011, **26**, 3450.
16 Y. Zhang, R. Yuan, Y.Q. Chai, W.J. Li, X. Zhong, H.A. Zhong, *Biosens. Bioelectron.*, 2011, 26, 3977.
17 M. Mallesha, R. Manjunatha, C. Nethravathi, G. S. Suresh, M. Rajamathi, J. S. Melo, T. V. Venkatesha, *Bioelectrochemistry,* 2011, **81**, 104.
18 C.Y. Deng, J.H. Chen, M.D. Wang, *Biosens. Bioelectron.*, 2009, **24**, 2091.
19 Y. Bao, J. Song, Y. Mao, D. Han, F. Yang, L. Niu, A. Ivaska, *Electroanalysis,* 2011, **23**, 878.
20 K. Esumi, K. Torigoe, *Colloid Polym. Sci.*, 2001, **117**, 80.
21 M.A. El-Sayed, *Acc. Chem. Res.,* 2001, **34**, 257.
22 L. Balogh, R. Valluzzi, K. S. Laverdure, S. P. Gido, G.L. Hagnauer,D. Tomalia, *J. Nanopart. Res.,* 1999, **1**, 353.
23 F. Gröhn, B.J. Bauer, Y.A. Akpalu, C.L. Jackson, E.J. Amis, *Macromolecules,* 2000, **33**, 6042.
24 K. Esumi, K. Miyamoto, T. Yoshimura, *J. Colloid Interface Sci.*, 2002, **254**, 402.
25 X. Shi, S. Wang, S. Meshinchi, M.E. Van Antwerp, *Small,* 2007, **3**, 1245.
26 P. Antoni, Y. Hed, A. Nordberg, D. Nyström, H. von Holst, A. Hult, M. Malkoch, *Angew. Chem. Int. Ed.*, 2009, **121**, 2160.
27 X. Peng, Q. Pan, G.L. Rempel, *Chem. Soc. Rev.*, 2008, **37**, 1619.
28 C.Q. Ma, E. Mena‐Osteritz, T. Debaerdemaeker, M.M. Wienk, R.A. Janssen, P. Bäuerle, *Angew. Chem. Int. Ed.*, 2007, **119**, 1709.
29 Y. Zhuo, G.F. Gui, Y.Q. Chai, N. Liao, K. Xiao, R. Yuan, *Biosens. Bioelectron.*, 2014, **53**, 459.
30 J. Han, Y. Zhuo, Y.Q. Chai, G.F. Gui, M. Zhao, Q. Zhu, R. Yuan, *Biosens. Bioelectron.*, 2013, **50**, 161.
31 M. Frasconi, C. Tortolini, F. Botre, F. Mazzei, *Anal. Chem.*, 2010, **82**, 7335.
32 A.S. Ramírez-Segovia, J.A. Banda-Alemán, S. Gutiérrez-Granados, A. Rodríguez, F.J. Rodríguez, Luis A. Godínez, E. Bustos, J. Manríquez, *Anal. Chim. Acta*, 2014, **812**, 18.
33 D. Zheng, J. Ye, L. Zhou, Y. Zhang, C. Yu, J. *Electroanal. Chem.,* 2009, **625**, 82.
34 A.X. Oliveira, S.M. Silva, F.R.F. Leite, L.T. Kubota, F.S. Damos, R. de Cássia Silva Luz, *Electroanalysis*, 2013, **25**, 723.